Role of Elemental Sublimation during Solution Heat Treatment of Ni-Based Superalloys

N. D'SOUZA, S. SIMMONDS, G.D. WEST, and H.B. DONG

The role of elemental evaporation on the microstructural stability of blade surfaces has been investigated on solutioned and aged samples of Ni-based single-crystal superalloys. Evaporation of Ni and Cr at the casting surface during solution heat treatment leads to the formation of a Ni- and Cr-depleted layer at the surface. Nucleation and growth of γ' phase occur within this layer through subsequent long-range diffusion of Re, Ta, and W between the γ' layer and the substrate. Beyond a critical Ni and Cr loss, incipient melting initiates at the surface and principally γ' and TCP phases are stabilized with de-stabilization of γ phase. Nucleation of TCP phases occurs at grain boundaries arising from cellular recrystallization during the ramp-up cycle. Therefore, on quenching, a range of microstructures are observed at the casting surface.

I. INTRODUCTION

SUPERALLOYS are a class of materials that have been specifically developed for high-temperature applications. The evolution from the 1st to 4th generation Ni-based superalloys has been motivated by the stringent demands on improved creep and fatigue resistance at elevated temperatures that is achieved by (1) increased solid solution strengthening and (2) the increased volume fraction of the precipitated γ' phases in the solid state. In order to achieve these goals, the alloys contain increasing amounts of refractory alloying elements such as Mo, Re, Ta, and W. The as-cast microstructure in the latest generation alloys is therefore associated with increasing levels of microsegregation and is consequently required to be heat treated to dissolve the low-melting interdendritic phases and to homogenize the microstructure.[1–7]

During solutioning, the alloy is heated above the γ'-solvus in the γ phase-field over a period of about 8 hours to homogenize the γ phase. However, recently, we have observed that microstructural instability develops across certain regions (that were scaled—NiO$_x$ surface oxide) of the aerofoil surface during solutioning,[8] the morphology of which is characteristic of a discontinuous reaction that shows a γ' matrix with TCP precipitates and γ-lamellae and the existence of a polycrystalline microstructure. This is unusual given that solutioning occurs within the γ phase-field. From the evolution of the microstructural instability at the surface of the aerofoil after heat treatment, it was deduced that Ni and Cr are

most likely lost *via* evaporation, thereby destabilizing the γ phase followed by redistribution of Re. However, certain key questions remain unexplained, specifically:

(a) It was observed that such microstructural instability only affected the scaled regions of the aerofoil (regions of the as-cast aerofoil covered with a NiO$_x$ scale, arising from transient oxidation due to mold/metal separation during casting,[9]) whereas regions that were unscaled are seen to be unaffected.
(b) During solutioning both oxidation and evaporation occur; however, the role of these two processes during solutioning on the microstructural instability is unknown.

The aim of the current study is therefore to examine the role of evaporation and oxidation on structural instability during solution heat treatment of Ni-based superalloys. The sequential evolution of the microstructure during solutioning and aging will be analyzed to reveal the role of elemental evaporation.

II. EXPERIMENTS

A. Sample Preparation and Solution Heat Treatment

In our experiments, cylindrical test bars (10-mm diameter and 6-cm height) of the 2nd generation Ni-based superalloy, CMSX4, was used because of the industrial importance and the nominal chemistry of CMSX4 is listed in Table I. Directional solidification was carried out at the Precision Casting Facility, Rolls-Royce, plc, Derby, UK, while heat treatment was carried out in a Schmetz furnace at Bodycote, Derby, UK. Details of the investment casting process have been summarized in a previous study; in this section, only details of the heat-treatment process will be presented.[8–10]

After casting, the test bar surfaces were grit-blasted with Al$_2$O$_3$ media to remove all surface oxides, including

N. D'SOUZA, Materials Technologist, is with the Rolls-Royce Plc, PO Box 31, Derby DE24 8BJ, U.K. S. SIMMONDS, Ph.D. Student, and H.B. DONG, Professor, are with the Department of Engineering, University of Leicester, Leicester LE1 7RH, U.K. Contact e-mail: h.dong@le.ac.uk G.D. WEST, Senior Research Fellow, is with the Department of Materials, Loughborough University, Leicestershire, LE10 2RF, U.K.

Table I. Calculated Composition (wt pct) Within 20 μm of the Surface Layer Following Ni, Co, and Cr Vaporization of Various Fractions of the Maximum Loss (Langmuir Equation) in Vacuum

Compositions (wt pct)	Ni	Al	Co	Cr	Ti	Mo	Ta	W	Re
NiO losses	59.90	5.89	9.65	6.6	1.12	0.61	6.6	6.6	3.05
20 pct Langmuir	50.25	9.77	6.47	3.70	1.85	1.01	10.95	10.95	5.05
15 pct Langmuir	54.78	8.47	7.68	3.21	1.61	0.88	9.50	9.50	4.38
10 pct Langmuir	58.25	7.48	8.61	2.83	1.42	0.77	8.38	8.38	3.87
8 pct Langmuir	59.43	7.15	8.92	2.70	1.36	0.74	8.01	8.01	3.70
5 pct Langmuir	61.00	6.70	9.34	2.53	1.27	0.69	7.50	7.50	3.46

Cr loss is maintained at 0.5 pct of the maximum, while Ni and Co fractional losses are varied.

NiO_x in scaled regions and Al_2O_3 in the unscaled regions. This is to ensure that the casting surface is thereafter oxide free to begin with. A thin layer of substrate material is also removed using grit blasting to remove surface eutectic since eutectic phase exists beneath the scaled layer. By doing this, the effects of as-cast oxides and eutectic phase on surface structure evolution can be excluded from our study so that effect of elemental evaporation on the sequential evolution of the microstructure during solutioning can be examined.

The test bars were then subsequently heat treated. Heat treatment consists of a solutioning and aging cycle. In the case of solutioning, a series of ramps and isothermal holds were used, and the final set temperature was 1585 K (1312 °C). The hold time at the set temperature was 8 hours. During ramp up, the initial vacuum level was 10^{-3} mBar (0.1 Pa). Beyond 1413 K (1140 °C), heating was done in an Ar atmosphere under an Ar pressure, $p_{Ar} = 0.5$ mBar (50 Pa). After solutioning, the test bars were rapidly gas fan quenched using Ar. Aging was done at 1413 K (1140 °C) for 2 hours under a vacuum level of 10^{-3} mBar (0.1 Pa) following which the test bars were rapidly gas fan quenched using Ar. In the case of the preoxidation measurements, a laboratory Carbolite furnace was used with a set temperature of 1373 K (1100 °C). The ramp rate was 10 K min^{-1}, and the hold time at temperature was 4 hours after which the bars were air cooled.

B. Microstructural Characterization

Aerofoil cross sections for microstructural characterization were prepared by initial grinding using SiC paper and a final polishing using 9 and 3 μm diamond pastes. For scanning electron microscopy (SEM) analysis including electron backscattered diffraction (EBSD), the samples received an extended additional mechano-chemical polish using a Vibromet with colloidal silica (0.65-μm particle size). All SEM analyses were performed using a dual beam (FEI Nova 600 nanolab). Backscattered electron imaging was undertaken using a retractable solid-state backscattered detector with accelerating voltages of 20 and 5 kV, with the latter providing images with the greatest channeling contrast for these samples. Kikuchi patterns for EBSD were collected using a Hikari camera (EDAX) and were indexed according to the Ni structure file at a rate of 280 frames s^{-1}. A beam voltage of 20 kV with a

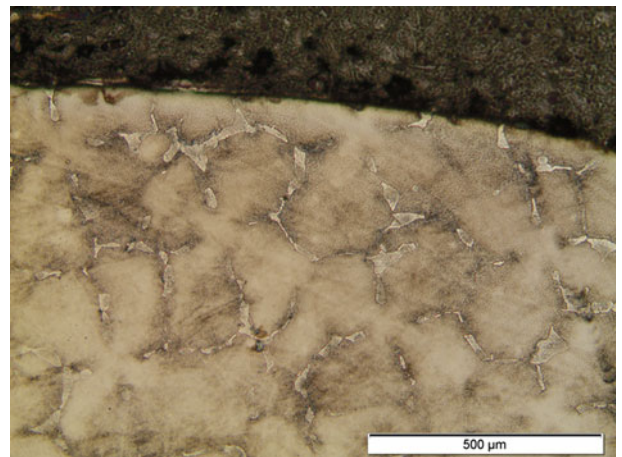Fig. 1—Optical micrograph (OM) showing the surface of the as-cast grit-blasted test bar before heat treatment. There is no existence of γ′ surface layer or visible oxide layer.

nominal current of 24 nA was employed to collect EBSD-derived maps. Orientation data were collected and analyzed using OIM software (version 5.31) from EDAX. Energy dispersive spectroscopy was also undertaken on the dual beam using an EDAX Apollo XL silicon drift detector. Spectra were collected from a minimum of three locations within a specified area of interest to check for consistency and possible subsurface features. All EDS spectra were collected at 20 kV under identical operating conditions: e.g., a nominal current of 2.3 nA, a working distance of 5 mm, an amplification time of 1.6 μs, and a live time of 30 seconds.

III. RESULTS AND DISCUSSION

A. Elemental Depletion in the Surface Layer of Solutioned Ni-based Alloys

Before heat treatment the as-cast and grit-blasted test bars were examined to assess the surface for any remaining oxides or eutectic. Figure 1 is an optical micrograph (OM) corresponding to a transverse section. It shows the interdendritic eutectic phases (i.e., γ′), but clearly, there is the absence of any eutectic decorating the surface. The dendrite lobes extend to the surface and any surface eutectic if present has spalled away following grit blasting. Sporadic islands of eutectic intersect the surface,
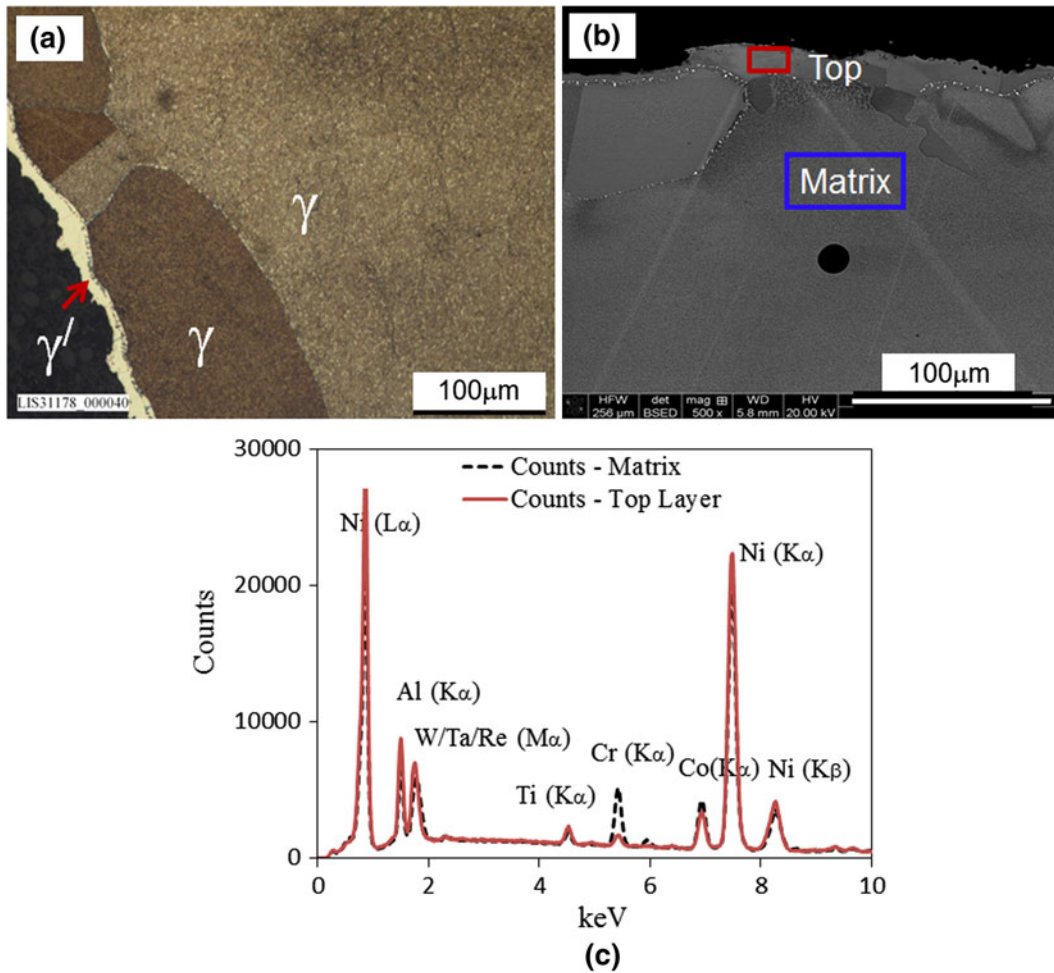
Fig. 2—Characterization of the γ' surface layer: (*a*) Optical micrograph (OM) showing γ' (*bright*) and recrystallized γ grains; (*b*) BEI showing surface morphology and area for compositional analysis; and (*c*) EDS from the surface layer and matrix.

but these are clearly very discrete but not continuous, as seen in Figure 1. Therefore, there is the conspicuous absence of the γ' surface layer before heat treatment.

Figure 2(a) is an OM that shows the microstructure that evolves across the surface of the test bars following solutioning and aging. Figure 2(b) is a backscattered electron image (BEI) that focuses in more detail on the surface layer, while Figure 2(c) is an energy dispersive analysis spectrum (EDS) that is collected from the surface layer and from the substrate. In Figure 2(c), the M-lines for Ta, W, and Re overlap as shown. The following observations can be made from Figures 2(a) through (c):

(i) There is an outer γ' layer that skirts the periphery of the test bars, which shows depletion in Cr, Co, and Ni. In some cases, γ grains nucleate from the γ' layer interface and grow into the substrate.
(ii) At the boundary between the γ' layer and the substrate, there is the nucleation of refractory-rich precipitates and their subsequent growth. This morphology is also observed sometimes at the boundaries between adjacent γ grains, or at the interface between γ grains and the substrate.

B. *Microstructure of the Ni/Cr-depleted γ' Surface Layer After Solutioning and Aging*

The BEIs in Figures 3(a) and (b) show the microstructures within the surface layers in more detail. The following observations can be made:

(iii) γ' Layer: Within the upper portion of this layer near the surface, there is the marked presence of pores, as we well as the existence of "specks" of refractory-rich precipitates; at the boundary with the substrate (or γ grains), there is the occurrence of discontinuous precipitation (DP) showing the nucleation and growth of refractory-rich precipitates and γ-lamellae.
(iv) γ Grains: It is clear that these grains constitute γ phase, with γ' precipitating in the solid state below the γ' solvus. DP is also sometimes observed at the boundary between neighboring γ grains.

The polycrystalline nature of the γ grains is evident from Figures 2 and 3; however, it is not known if the γ' surface layer is polycrystalline. Figure 4(a) is a BEI and the accompanying EBSD-derived inverse pole figure

(IPF) map corresponding to this region is presented in Figure 4(b). While the polycrystalline nature of γ grains is indicated, importantly, it can be unequivocally ascertained that the γ' surface layer is also polycrystalline. In fact, this can be also deduced from the BEI in Figure 3(a), where the distinct contrast within the surface layer in addition to being composition dependent, also has a crystallographic contribution, which is enhanced at low voltage. While the formations of the polycrystalline γ' surface layer and γ grains occur during solutioning, the DP reaction is most likely to occur during aging, since it is grain boundary diffusion controlled. To conclusively ascertain that this is the case, only solutioned (unaged) samples were considered.

A typical BEI corresponding to this condition is shown in Figure 5. It is can be observed that while the microstructures within the γ' surface layer and γ grains are similar to that observed after aging, there is the distinct absence of DP throughout the microstructure. However, there is the occurrence of refractory-rich precipitates at the grain boundary separating the γ' surface layer from the substrate.

C. Microstructure and Chemistry in Surface Layer after Preoxidation

The stabilization of γ' at the surface requires the removal of γ stabilizers—most notably Cr and Re; the
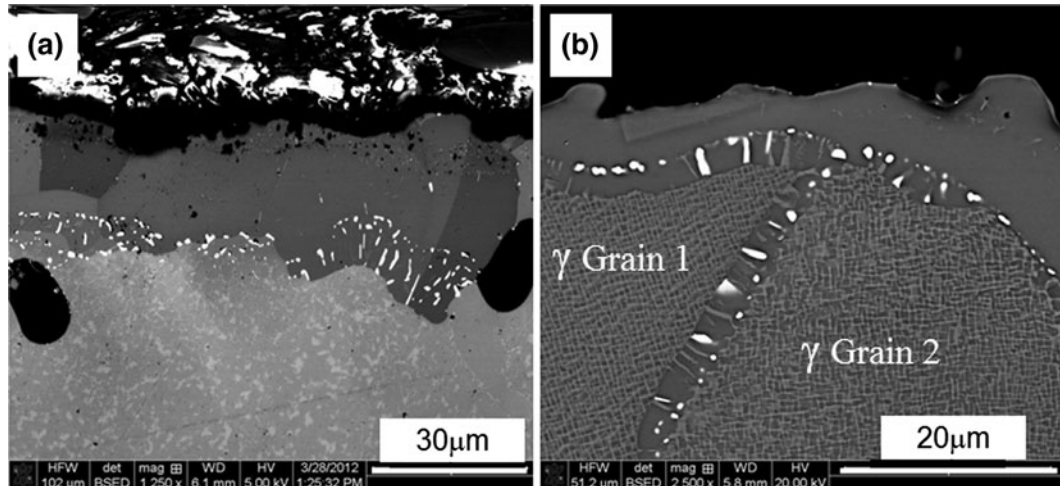

Fig. 3—Characterization of the γ' surface layer: (a) BEI (5kV) showing some grain orientation contrast in the surface layer as well as evidence of DP involving nucleation and growth of refractory-rich precipitates always observed at the interface between γ' surface layer and substrate, (b) BEI (20kV) showing DP also observed sometimes between neighboring recrystallized γ grains.
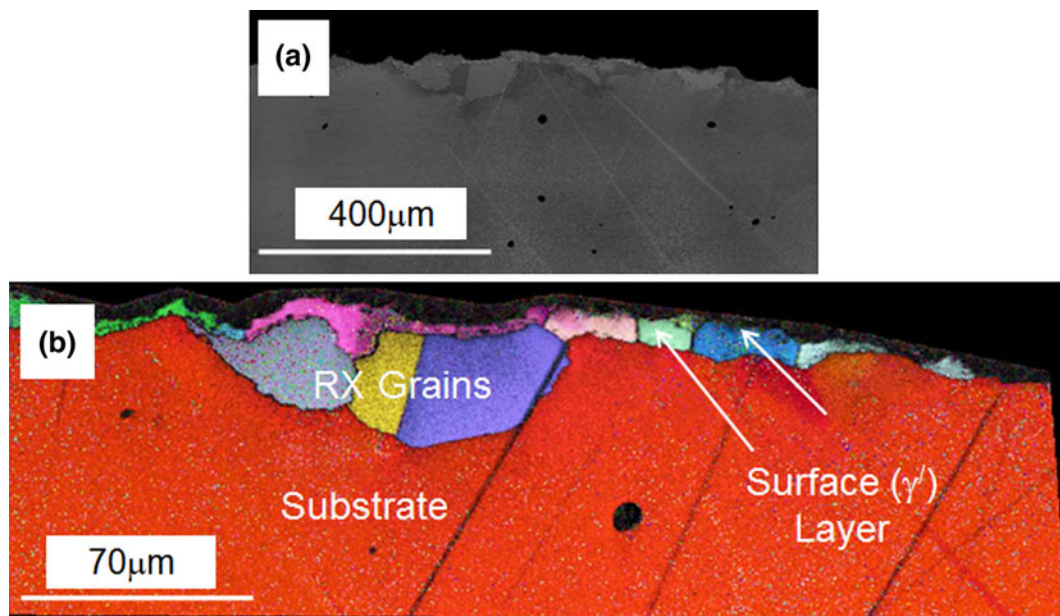

Fig. 4—Crystallographic characterization of the γ' surface layer: (a) BEI showing surface layer, recrystallized grains and substrate; and (b) Orientation-derived IPFs map (IPM) using electron backscattered diffraction (EBSD).
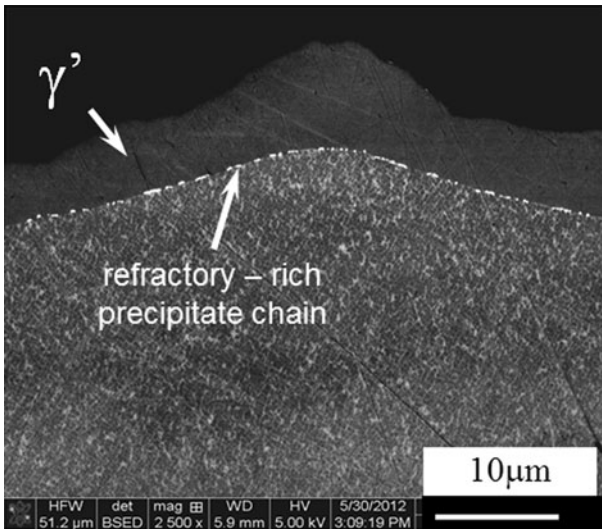
Fig. 5—BEI image of γ′ surface layer, substrate, and nucleated refractory-rich precipitates after solutioning (not aging).
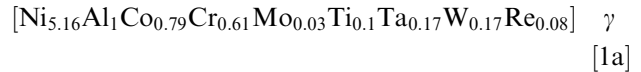
depletion of Cr in γ′ is observed in Figure 2(c). Therefore, one of the ways for suppressing the formation of the γ′ surface layer is to stabilize γ-forming elements at the surface. This can be achieved by preoxidation. Figure 6(a) is a BEI that shows the microstructure in a preoxidized test bar. Three distinct regions can be identified: (1) the outermost layer that shows internal oxidation, (2) an intermediate γ′ denuded layer, and (3) the substrate beneath. There is an important and a significantly different response of the surface morphologies that subsequently develop during solutioning of the preoxidized test bars. Figure 6(b) shows the surface morphology of the preoxidized test bar following solutioning, while Figure 6(c) compares EDS spectra collected from the surface layers and the substrate. In Figure 6(c), the M-lines for Ta, W, and Re overlap as shown, however, these peaks can be successfully deconvoluted in most cases. There is the marked absence of the polycrystalline γ′ surface layer; as seen in Figure 6(b) and confirmed by the spectra collected from the surface layer and the substrate, where the numbers of counts for the individual elements are identical. However, there is clear evidence of internal oxidation showing the presence of internal islands of Al_2O_3, which appear as a black chain in Figure 6(b). Therefore, by producing a layer "locally" stabilized in γ phase (reduced in Al) and therefore having a lower γ′-solvus temperature, it is possible to preclude the formation of the γ′ surface layer.

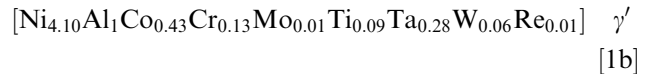### D. Elemental Evaporation from the Surface During Solutioning and Evolution of Surface Microstructures

As described previously, solutioning was carried out in the γ-phase field, when the as-cast eutectic progressively dissolves and the microstructure is homogenized by long-range diffusion, while, at the surface, oxidation occurs with the formation of Al_2O_3.[10] Growth of Al_2O_3 should be accompanied by progressive depletion of Al at the surface leading to a γ′-denuded zone, the extent of

which is dependent on the oxide growth rate and the rate of Al diffusion from the substrate. The typical oxide thickness in the heat-treated condition is from 1 to 2 μm; however, the heat-treated alloy exhibits an increasing stabilization of γ′ beneath the oxide (Figures 2(a) and (b)). The stabilization of γ′ requires significant solute redistribution within the surface layers.

For the nominal composition, γ phase can be written as

$$[Ni_{5.16}Al_1Co_{0.79}Cr_{0.61}Mo_{0.03}Ti_{0.1}Ta_{0.17}W_{0.17}Re_{0.08}] \quad \gamma \quad [1a]$$

On the other hand, γ′ phase can be written as

$$[Ni_{4.10}Al_1Co_{0.43}Cr_{0.13}Mo_{0.01}Ti_{0.09}Ta_{0.28}W_{0.06}Re_{0.01}] \quad \gamma' \quad [1b]$$

Stabilization of γ′ phase requires a decrease in the Ni/Al ratio and also removal of principal solute species Re, W, and Cr. However, Ni, Co, and Cr are characterized by high vapor pressures, compared with other solute species, and therefore the role of sublimation needs to be considered. The equilibrium partial pressures in atm for Ni, Co, and Cr are given elsewhere[11]

$$\log[p_{Ni}] = 10.557 - \frac{22606}{T} - 0.8717\log T \quad [2a]$$

$$\log[p_{Cr}] = 6.800 - \frac{20733}{T} + 0.4391\log T \quad [2b]$$

$$\log[p_{Co}] = 10.976 - \frac{22576}{T} - 1.028\log T \quad [2c]$$

However, in the case of solid solutions and assuming ideal behavior, Raoult's law applies, and the partial pressure is proportional to the mole fraction. The rate of vaporization in vacuum is proportional to the partial pressure and is given by the modified Langmuir equation;[12]

$$E = \frac{p}{\sqrt{2\pi MRT}} \quad [3]$$

where E is the number of moles evaporated per square meter per second, p is the vapor pressure, and M is the molecular weight.

Figure 7(a) expresses the mass loss rates using Eq. [3] for vaporization into vacuum for Ni, Co, and Cr, which has been scaled for mole concentration according to Raoult's law. Cr losses are at least one order of magnitude greater compared with Ni and Co. For the dimensions of the test bar (10-mm diameter and 60-mm length) and for a solutioning time of 8 hours, the number of moles of Ni, Co, and Cr vaporized were calculated from which the mass loss can be determined. The Langmuir equation considers evaporation into vacuum. However, vaporization of elements in our experiments occurs under Argon atmosphere, thus fractional losses of the total Langmuir
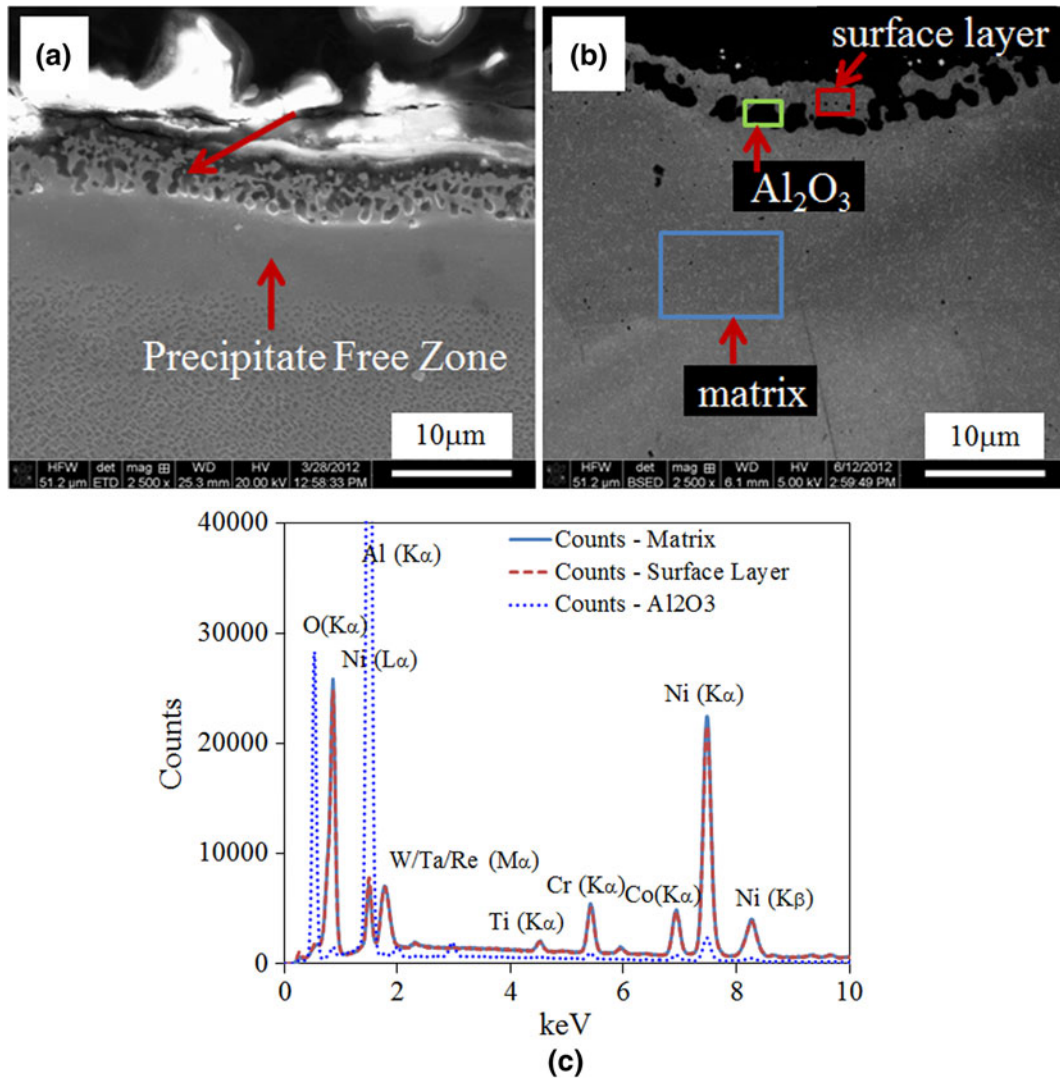
Fig. 6—Characterization of the γ' surface layer: (a) BEI showing surface morphologies in preoxidized specimen, (b) BEI following solutioning, and (c) EDS from surface layers and matrix.
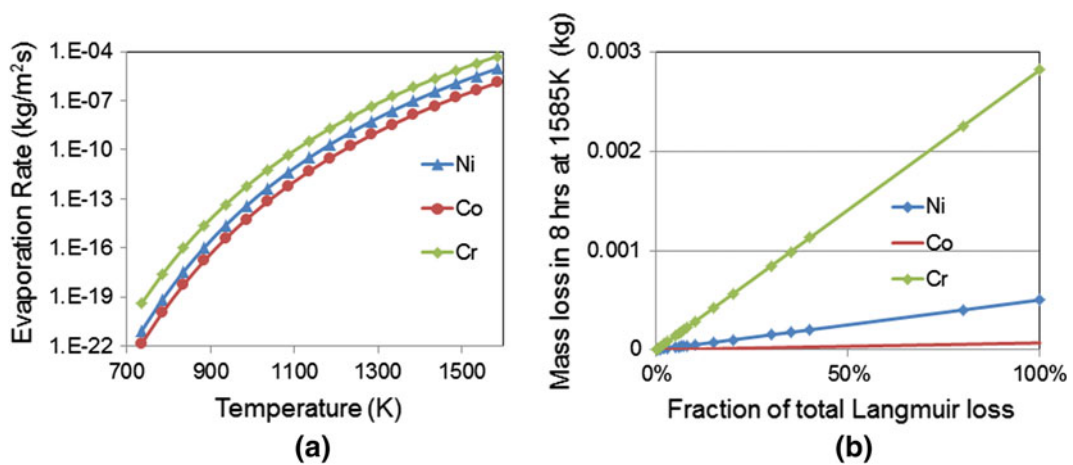

Fig. 7—(a) Mass loss rates of Ni, Co, and Cr from the sample surface (10 mm in diameter and 60 mm in length) using Langmuir equation (b) Mass loss (kg) of Ni, Co, and Cr from the sample surface during 8 h solutioning at 1585 K for different pct's of total Langmuir loss.

loss shall be assumed. These Langmuir mass loss fractions are illustrated in Figure 7(b). This will be used as a basis in the subsequent calculations where the evolution of phases within the substrate at the surface will be calculated for different fractions of the Langmuir loss.

From Figures 2 and 3, the thickness of the surface layer was between 20 and 30 μm in thickness. Therefore, we assume that any Ni loss by vaporization originates from the 20-μm-thick γ′ surface layer during solutioning. This tacitly neglects any interaction of this surface layer with the bulk substrate and is a reasonable first approximation. We only consider Ni, Co, and Cr losses, since these elements have the greatest vapor pressures and only their losses are significant.[11] Cr loss is estimated at 0.5 pct of Langmuir which, within the 20 μm γ′ layer surface, equates to 0.01 g, whereas the total mass of Cr in the surface layer is only 0.02 g. 1 pct of Langmuir loss, or higher, removes more Cr than the total amount of Cr within that layer since Cr has a high vapor pressure. At the solutioning temperature of 1585 K (1312 °C) therefore, corresponding to these fractions of elemental losses, the wt pct of all elements was then recalculated. Details are listed in Table I. Subsequently, by means of a commercial software database, ThermoCALC,[13] it is possible to determine the phase evolution. When liquid is predicted at the solutioning temperature, a Scheil solidification profile (i.e., the absence of backdiffusion) was used to model the quench process. However, since freezing eventually terminates with limited backdiffusion, phase fractions were calculated when the remnant liquid fraction

reaches 10 pct. Calculated transition temperature and phase fractions are listed in Tables II and III. For a comparison, the concentration changes in the 20-μm surface layer because of the formation of the NiO scale layer (~0.5 μm thick) are listed as NiO losses in Table I. For NiO loss predictions, only the Ni loss is considered, and there are no losses of other elements.

The solutioning temperature [1585 K (1312°C)] corresponds to the γ-phase field for the nominal composition, where there is complete dissolution of the γ′. However, for Ni, Co losses greater than 8 pct of the Langmuir value (0.040 and 0.006 g, respectively) and Cr losses of 0.5 pct of the Langmuir value (0.01 g), this results in incipient melting and TCP phase formation. The phase evolution for representative fractional losses in Table II is graphically illustrated in Figures 8(a) through (d), showing that for fractional losses of 10 pct and more for Ni and Co (0.5 pct loss for Cr), the dissolution of γ occurs at 1473 K (1200 °C) with increasing amounts of NiAl and TCP phases (σ, μ) being stabilized.

An added complication arises when solutioning is carried out in the presence of Ar. Oxidation occurs, and this is to be expected given the large negative free energy of formation of oxides of Al, Ni, and Cr.[14] Under equilibrium conditions, the oxygen partial pressure (p_{O_2}) can be determined, above which oxidation of any species is thermodynamically favorable. Taking into account solid-solution aspects, rather than pure elements and ideal solution behavior, the standard free energy for the oxidation reaction is

Table II. Calculated Transition Temperatures for Alloy Compositions with Different Fraction Losses in the Surface Layer

Fractions of Langmuir Loss	Nominal Composition	NiO Losses	5 pct Ni, Co 0.5 pct Cr	8 pct Ni, Co 0.5 pctCr	10 pct Ni, Co 0.5 pctCr	15 pct Ni, Co 0.5 pctCr	20 pct Ni, Co 0.5 pctCr
Liquidus °C	1369	1362	1374	1362	1382	1464	1559
Solidus °C	1329	1324	1331	1314	1298	1263	1241
γ′ solvus °C	1260	1265	1331	1329	1324	1311	1272

Table III. Phases (mole pct) Present at 1312 °C Hold and After Quench Calculated Using ThermoCALC Under Scheil Solidification Condition

Fractions of Langmuir loss	Nominal CMSX4 Alloy	NiO Losses	5 pct Ni, Co 0.5 pct Cr	8 pct Ni, Co 0.5 pctCr	10 pct Ni, Co 0.5 pctCr	15 pct Ni, Co 0.5 pctCr	20 pct Ni, Co 0.5 pctCr
Phases at 1312 °C (equilibrium condition)	γ (100 pct)	γ (100 pct)	γ (73.6 pct) γ′ (26.4 pct)	γ (58 pct) γ′ (41.2 pct) σ (8 pct)	Liquid (19 pct) γ′ (44 pct) γ (35 pct) σ (2 pct)	Liquid (87 pct) γ′ (11 pct) σ (2 pct)	Liquid (65.9 pct) NiAl (29.4 pct) σ (3.8 pct) BCC_A2(0.9 pct)
Phases after quenching (Scheil condition is assumed for solidifying the remelt liquid)	n/a	n/a	n/a	n/a	At 1195°C γ′ (79 pct) γ (17 pct) σ (2 pct) NiAl (1 pct) P (1 pct)	At 1214°C γ′ (56.4 pct) NiAl (20 pct) σ (2.4 pct)	At 1173°C γ (24.8 pct) γ′ (23 pct) NiAl (47 pct) σ (4.2 pct) BCC_A2 (1 pct)
Equilibrium phases	Nominal CMSX4 alloy				At 1195°C γ (72 pct) γ′(28 pct)	At 1214°C γ (78 pct) γ′ (22 pct)	At 1173°C γ (64.9 pct) γ′ (34.8 pct) P (0.3 pct)

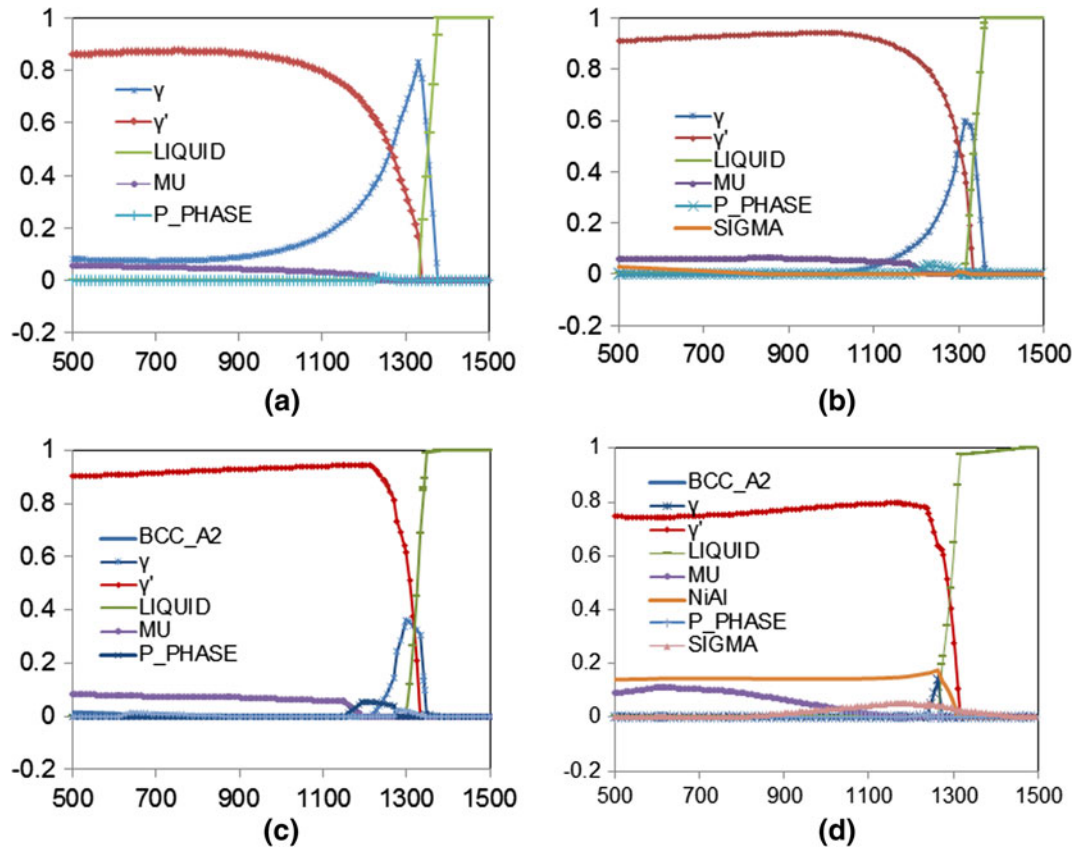Equilibrium condition was assumed for nominal CMSX4 alloy.

Fig. 8—Phase evolution calculated using ThermoCALC under equilibrium condition[13] for elemental losses (*a*) 5 pctLangmuir Ni,Co loss; (*b*) 8 pct Langmuir Ni,Co loss; (*c*) 10 pct Langmuir Ni,Co loss; (*d*) 15 pct Langmuir Ni,Co loss. Cr Langmuir losses are at 0.5 pct for (*a*) through (*d*).

$$G^0 = -RT\ln\left[\frac{1}{X_i p_{O_2}}\right] \qquad [5]$$

where, X_i refers to the mole fraction of the *i*th species. Cr is much more readily oxidized than Ni, given that p_{O_2} (Cr) $\ll p_{O_2}$ (Ni). The oxide presents a physical barrier to the sublimation of species from the surface and is greater for denser oxides, such as Al_2O_3.

In an earlier study, it has been shown that transient oxidation dominates following mold/metal separation during casting, where the surface of the aerofoil that has "pulled" away from the mold wall oxidizes to NiO_x. This "scaled" NiO_x surface constitutes the transient oxidation product; despite Al_2O_3 being the more stable oxide, it is absent in this region.[9] During initial transient oxidation, growth kinetics dominates, and the growth kinetics of NiO_x is two-orders of magnitude greater than Al_2O_3, owing to its porous nature. It is, however, important to note that the typical pressure in the casting furnace is 7×10^{-7} atm and therefore, p_{O_2} is at most 1.4×10^{-7} atm (20 pct). The mechanism for the formation of surface scale operates only at lower temperatures; typically lower than 1473 K (1200 °C).[9] It is clear therefore from Figure 7(a) that the formation of NiO_x is to be expected, since, p_{O_2} (furnace) > p_{O_2} (critical) ~10^{-9} atm. However, in the current study, the test bars are grit blasted, and any surface oxide present after casting is mechanically stripped away to leave an initial unoxidized surface. Therefore, during subsequent ramp-up and isothermal hold during solutioning, both elemental sublimation and oxidation will occur. The oxide observed on the surface of the test bar after solutioning is Al_2O_3, with the distinctive absence of NiO_x. The key consideration during solutioning is that unlike casting, this is carried out in the presence of Ar under a partial pressure of 5×10^{-4} atm. The formation of NiO_x is significantly reduced at higher temperatures by the low p_{O_2} (~10^{-8} atm) and its ease of reduction by CO/CO_2 within the heat-treatment furnace.[15] Only Cr_2O_3 and other volatile oxides of Cr, such as CrO_3 and CrO_2, will form along with Al_2O_3.[16] The latter is the most stable oxide with the slowest growth kinetics and forms beneath the outer oxides.

Despite the formation of NiO_x being minimal owing to thermodynamic considerations, as discussed before, it is still instructive to ascertain the implications of the loss of Ni to form the oxide and the subsequent microstructural instability that might be expected following from calculations listed in Tables II and III. The typical oxide thickness was 0.5 μm and assuming stoichiometry of NiO, there is only marginal change in the composition (Table II). From Table II, the calculated solidus temperature was 1597 K (1324 °C), and γ phase is stable at the solutioning temperature. Therefore, oxidation leading to NiO_x cannot account for the surface microstructural instability observed.

It is beyond the scope of this article to quantitatively describe the vaporization losses with the evolution of the oxide scale, and this is the topic of ongoing research by this author group; however, it suffices to qualitatively demonstrate unequivocally this key phenomenon that occurs during solutioning and the precursor to the evolution of the surface microstructures. The results on the preoxidized and solutioned test bars adequately support the role of sublimation. In the preoxidized test bars, there is the formation of the precipitate-free zone (PFZ) as well as the clear evidence of internal oxidation following isothermal oxidation. There is the formation of a dense Al_2O_3 layer on the surface, as well as an Al-depleted surface layer (PFZ; ~10 μm) (Figure 6(a)). The dense Al_2O_3 layer that is present at the outset presents a physical barrier to sublimation, while the depleted Al at the surface corresponds to a lowered γ' solvus temperature for the surface layer. Both these factors mitigate the propensity to form the γ' surface layer during solutioning. This is consistent with the surface morphology in Figure 6(b), which shows the marked absence of the γ' layer. Furthermore, the spectrum from the surface layer shows that this is γ phase, having similar solute partitioning as the matrix (Figure 6(c)).

Evaporation of Ni and Cr from the surface would result in a decrease in Ni/Al ratio; Eqs. [1a] and [1b]. At solutioning temperatures, $\frac{T}{T_M} > 0.75$, volume diffusion is predominant; however, as observed for all Ni losses exceeding 10 pct of the maximum Langmuir loss, incipient melting is predicted to occur at the surface. In addition, there is also the occurrence of TCP phases (P-phase) and also β-NiAl for Ni losses approaching up to 20 pct of the maximum loss. However, the latter has not been observed, thereby indicating that Ni losses are not of those levels. Therefore, sublimation of Ni and Cr from the surface is compensated by diffusion of Ni and Cr from the substrate through the layer of thickness of t to the surface, which is composed of L, γ, γ', and TCP phases depending on the extent of Ni loss. It is clear that diffusion through the liquid is at least four orders of magnitude greater than that through γ phase. This results in the "affected" surface layer ingressing by an incremental thickness dt into the substrate, i.e., the coupling of vaporization and interdiffusion with the substrate.

The nucleation of the TCP phases within grains is impeded by a high nucleation barrier and is often associated with significant annealing times (TTT diagram governed).[17–19] Alternatively, nucleation is more profuse in the presence of grain boundaries, which acts as potent nucleation sites, such as in DP,[20–22] or in the case of the secondary reaction zone observed beneath coatings associated with diffusion of Al from the coating to the substrate and Ni in the opposite direction.[19,23,24] However, abrasive grit blasting induces damage along the surface of the material. The damage in the form of localized strain results in recrystallization. This has been observed in interrupted solutioning experiments at temperatures below the γ' solvus. An interrupted experiment at 1200 °C showed a typical cellular morphology, i.e., γ' matrix with TCP precipitates and γ-lamellae. This is akin to the microstructure observed during aging and

corresponds to the classical cellular recrystallization morphology. The grain boundary migrates through the γ/γ' microstructure and is accompanied by local dissolution of the γ' ahead of the boundary. Once the boundary passes through, γ' reprecipitates within the grain behind the boundary. This is energetically more favorable than cutting of the precipitates, since coherency with the γ phase would be lost and is therefore not energetically favorable.[25–27] Following the passage of the grain boundary, there would be progressive coarsening of the γ phase within the grain, resulting in the characteristic cellular recrystallization morphology, involving γ-lamellae. The vapor pressures are an order of magnitude lower at 1473 K (1200 °C) compared with the solutioning temperature of 1585 K (1312 °C), implying that vaporization is significantly retarded at the lower temperature. Consequently, following vaporization and incipient melting, the existing grain boundaries within the unmolten portion of the surface, will act as nucleation sites for the nucleation of TCP phases, as dictated by the equilibrium phase fraction at the solutioning temperature.

On the other hand, as observed in Figures 4(a) and (b), there is the occurrence of γ recrystallized grains ahead of the γ' surface layer into the substrate. Importantly, there is a distinct grain boundary both between the γ' surface layer and the recrystallized grain, as well as between the recrystallized grain and the substrate. The latter is easily attributed to recrystallization, but the former requires explanation. It is clear therefore that the γ' surface layer precedes the recrystallized grain; otherwise the occurrence of the grain boundary between the γ' surface layer and the recrystallized grain cannot be accounted for. The nucleation of the γ recrystallized grain occurs at the interface of the molten surface layer and the unmolten substrate. Growth of this grain occurs through the matrix and is dependent on accumulated plastic strain. Subsequent freezing of the liquid at the surface via a "chilling" effect during quenching after solutioning results in the nucleation of grains with random orientation resulting in predominantly γ' morphology. This has been modeled via a Scheil analysis and the phases listed in Table III.

IV. CONCLUSIONS

(1) The role of sublimation and its implications on surface microstructural stability during solutioning and aging of Ni-based alloys has been examined, with specific reference to the alloy, CMSX4.
(2) The evaporation of principally Ni and Cr leads to the formation of a Ni- and Cr-depleted layer near surface; nucleation and growth of γ' phase occur within the layer through subsequent long-range diffusion of (a) Ni and Cr from the γ' layer/substrate interface to the surface, and (b) that of Re and W from the γ' layer/substrate interface into the substrate.
(3) Beyond a critical Ni and Cr loss, incipient melting initiates at the surface, and principally γ' and TCP phases are stabilized with de-stabilization of γ

phase. Nucleation of TCP phases occurs at grain boundaries arising from cellular recrystallization during the ramp-up cycle. Therefore, on quenching, a range of microstructures are observed at the casting surface.

(4) Therefore, the conventional design of heat-treatment protocols to dissolve the as-cast eutectic and to homogenize the bulk microstructure is clearly not complete without addressing the microstructure instability at the casting surface.

REFERENCES

1. H.T. Pang, H.B. Dong, R. Beanland, H.J. Stone, C.M.F. Rae, P.A. Midgley, G. Brewster, and N. D'Souza: *Metall. Mater. Trans. A*, 2009, vol. 40A, pp. 1660–69.
2. N. D'Souza and H.B. Dong: *Scripta Mater.*, 2007, vol. 56, pp. 41–44.
3. N. D'Souza and H.B. Dong: *Mat. Sci. Tech*, 2011, vol. 27, pp. 325–31.
4. S.-M. Seo, J.-H. Lee, Y.-S. Yoo, C.-Y. Jo, H. Miyahara, and K. Ogi: in *Superalloys 2008*, R.C. Reed, K.A. Green, P. Caron, T.P. Gabb, M.G. Fahrmann, E.S. Huron, and S.A. Woodard, eds., TMS, Warrendale, PA, 2008, pp. 277–86.
5. G.E. Fuchs: *Mater. Sci. Eng. A*, 2001, vol. 300A, pp. 52–60.
6. N. Warnken, H. Larrson, and R.C. Reed: *Mater. Sci. Technol.*, 2009, vol. 25, pp. 179–85.
7. S.L. Semiatin, R.C. Kramb, R.R. Turner, F. Zhang, and M.M. Anthony: *Scripta Met.*, 2004, vol. 51, pp. 491–95.
8. N. D'Souza, G.D. West, G. Brewster, H.B. Dong, and B.A. Shollock: unpublished research.
9. G. Brewster, N. D'Souza, K. Ryder, S. Simmonds, and H.B. Dong: *Metall. Mater. Trans. A*, 2012, vol. 43A, pp. 1288–1302.
10. J.J. Gyaneshwara: Ph.D. Thesis, University of Cambridge, UK, 2009.
11. C.B. Alcock, V.P. Itken, and M.K. Horrigan: *Can. Met. Quart.*, 1984, vol. 23, pp. 309–13.
12. L.D. Jaffe and J.B. Rittenhouse: *Evaporation of Materials in Space, Technical Report 32–161*, Jet Propulsion Laboratory, California Institute of Technology, Pasadena, CA, 1961, pp. 32–161.
13. Thermo-Calc Software, NIDAT7 Ni-based superalloy database. http://www.thermocalc.com. Accessed Feb 2013.
14. F.D. Richardson and J.H.E. Jeffes: *J. Iron Steel Inst.*, 1948, vol. 160, pp. 261–70.
15. D.R. Gaskell: *Introduction to Metallurgical Thermodynamics*, 1981, McGraw-Hill Series in Materials Science and Engineering Hemisphere Pub. Corp, 1981, ISBN: 0070229465, 9780070229464.
16. R.T. Grimley, R.P. Burns, and M.G. Ingram: *J. Chem. Phys.*, 1961, vol. 32, pp. 664–67.
17. R. Darolia, D.F. Lahrman, and R.D. Field: in *Superalloys 1988*, S. Reichman, D.N. Duhl, G. Maurer, S. Antolovich, and C. Lund, eds., TMS, Warrendale, 1988, pp. 255–64.
18. S. Tin and T.M. Pollock: *Mat. Sci. Eng.*, 2003, vol. A348, pp. 111–121.
19. C.M.F. Rae and M.S. Hook: *R. C. Reed*, 2005, vol. A396, pp. 231–39.
20. J.D. Nystrom, T.M. Pollock, W.H. Murphy, and A. Garg: *Metall. Mater. Trans. A*, 1997, vol. 28A, pp. 2443–52.
21. A. Heckl, S. Cenanovic, M. Goken, and R.F. Singer: *Acta Mater.*, 2011, vol. 59, pp. 6563–73.
22. A. Heckl, S. Cenanovic, M. Goken, and R.F. Singer: *Metall. Mater. Trans. A*, 2012, vol. 43A, pp. 10–19.
23. A. Suzuki, C.M.F. Rae, M. Yoshida, Y. Matsubara, and H. Murakami: in *Superalloys 2008*, R.C. Reed, K.A. Green, P. Caron, T.P. Gabb, M.G. Fahrmann, E.S. Huron, and S.A. Woodard, eds., TMS, Warrendale, 2008, pp. 777–85.
24. W.S. Walston, J.C. Schaeffer, and W.H. Murphy: in *Superalloys 1996*, R.D. Kissinger, D.J. Deye, D.L. Anton, A.D. Cetel, M.V. Nathal, T.M. Pollock, and D.A. Woodford, eds., TMS, Warrendale, 1996, pp. 9–18.
25. A. Porter and B. Ralph: *J. Mater. Sci.*, 1981, vol. 16, pp. 707–13.
26. J.M. Oblak and W.A. Owczarski: *Trans. Metall. Soc., AIME*, 1968, vol. 242, pp. 1563–68.
27. R. Brugel, P.D. Portella, and J. Preuhs: in *Superalloys 2000*, T.M. Pollock, R.D. Kissinger, R.R. Bowman, K.A. Green, M. McLean, S. Olson, and J.J. Schirra, eds., TMS, Warrendale, PA, 2000, pp. 229–38.